Chemical Science

ROYAL SOCIETY OF CHEMISTRY

EDGE ARTICLE

View Article Online
View Journal | View Issue

Check for updates

Cite this: *Chem. Sci.*, 2024, **15**, 4960

All publication charges for this article have been paid for by the Royal Society of Chemistry

Open Access Article. Published on 29 February 2024. Downloaded on 2/8/2026 11:43:49 AM. This article is licensed under a Creative Commons Attribution 3.0 Unported Licence.

Infrared spectroscopy reveals metal-independent carbonic anhydrase activity in crotonyl-CoA carboxylase/reductase†

Aharon Gomez, ‡§[a] Matthias Tinzl,§[b] Gabriele Stoffel,[b] Hendrik Westedt,[b] Helmut Grubmüller,[c] Tobias J. Erb,[bd] Esteban Vöhringer-Martinez *[a] and Sven T. Stripp *[ef]

Received 11th August 2023
Accepted 27th February 2024

DOI: 10.1039/d3sc04208a

rsc.li/chemical-science

The conversion of CO_2 by enzymes such as carbonic anhydrase or carboxylases plays a crucial role in many biological processes. However, *in situ* methods following the microscopic details of CO_2 conversion at the active site are limited. Here, we used infrared spectroscopy to study the interaction of CO_2, water, bicarbonate, and other reactants with β-carbonic anhydrase from *Escherichia coli* (*Ec*CA) and crotonyl-CoA carboxylase/reductase from *Kitasatospora setae* (*Ks*Ccr), two of the fastest CO_2-converting enzymes in nature. Our data reveal that *Ks*Ccr possesses a so far unknown metal-independent CA-like activity. Site-directed mutagenesis of conserved active site residues combined with molecular dynamics simulations tracing CO_2 distributions in the active site of *Ks*CCr identify an 'activated' water molecule forming the hydroxyl anion that attacks CO_2 and yields bicarbonate (HCO_3^-). Computer simulations also explain why substrate binding inhibits the anhydrase activity. Altogether, we demonstrate how *in situ* infrared spectroscopy combined with molecular dynamics simulations provides a simple yet powerful new approach to investigate the atomistic reaction mechanisms of different enzymes with CO_2.

Introduction

Developing catalytic strategies for the capture and conversion of carbon dioxide (CO_2) is key to increased mitigation, utilization, and sequestration of this critical greenhouse gas. While still being a challenge for synthetic chemistry enzymes provide a natural blueprint for efficient CO_2-converting catalysts.[1] Several enzymes are known that interact with CO_2 and/or bicarbonate (HCO_3^-) during catalysis, in particular carbonic anhydrases (CAs) and carboxylases.

CAs catalyze the reversible conversion of CO_2, H_2O, and bicarbonate (HCO_3^-) with rate enhancements of close to 8×10^6 compared to the reaction in aqueous solution (eqn (1)). This makes them one of the most effective CO_2-converting catalysts in nature.[2] CAs are present in all three domains of life and have been classified in eight families.[3] Almost all known CAs feature a zinc cation (Zn^{2+}) as active site cofactor,[4] which plays a central role in catalysis as Zn^{2+} coordinates a hydroxide anion (OH^-) that attacks CO_2 as a nucleophile to form HCO_3^- (Scheme 1). The OH^- species itself is generated through proton abstraction from a zinc-bound water molecule to a nearby base, which is usually a histidine.[5–8]

$$CO_2 + 2H_2O \leftrightarrow HCO_3^- + H_3O^+ \quad (1)$$

Carboxylases catalyze the addition of CO_2 to an acceptor substrate with the family of enoyl-CoA carboxylases/reductases (ECRs) encompassing some of the most efficient CO_2-fixing enzymes found in nature.[9] ECRs catalyze the reductive carboxylation of α,β-unsaturated enoyl-CoAs with the reduced form of nicotinamide adenine dinucleotide phosphate (NADPH) as cofactor. Hydride transfer from NADPH to the enoyl-CoA substrate generates a reactive enolate species, which acts as a nucleophile that attacks a CO_2 molecule bound at the active site.[10,11] At the example of crotonyl-CoA carboxylase/reductase from *Kitasatospora setae* (*Ks*Ccr), Fig. 1 illustrates how CO_2-

[a]*Departamento de Físico Química, Facultad de Ciencias Químicas, Universidad de Concepción, Concepción, Chile. E-mail: evohringer@udec.cl*

[b]*Department of Biochemistry and Synthetic Metabolism, Max-Planck-Institute for Terrestrial Microbiology, Karl-von-Frisch-Str. 10, D-35043 Marburg, Germany*

[c]*Department of Theoretical and Computational Biophysics, Max-Planck-Institute for Multidisciplinary Sciences, Am Fassberg 11, 37077 Göttingen, Germany*

[d]*Center for Synthetic Microbiology (SYNMIKRO), Germany*

[e]*Freie Universität Berlin, Experimental Molecular Biophysics, Arnimallee 14, 14195 Berlin, Germany*

[f]*Technische Universität Berlin, Division of Physical Chemistry, Strasse des 17. Juni 124, 10623 Berlin, Germany. E-mail: s.stripp@tu-berlin.de*

† Electronic supplementary information (ESI) available. See DOI: https://doi.org/10.1039/d3sc04208a

‡ Present address: Departamento de Ciencias Biológicas y Químicas, Facultad de Medicina y Ciencia, Universidad San Sebastián, Concepción, Chile.

§ These authors contributed equally.

© 2024 The Author(s). Published by the Royal Society of Chemistry

Open Access Article. Published on 29 February 2024. Downloaded on 2/8/2026 11:43:49 AM.
This article is licensed under a Creative Commons Attribution 3.0 Unported Licence.

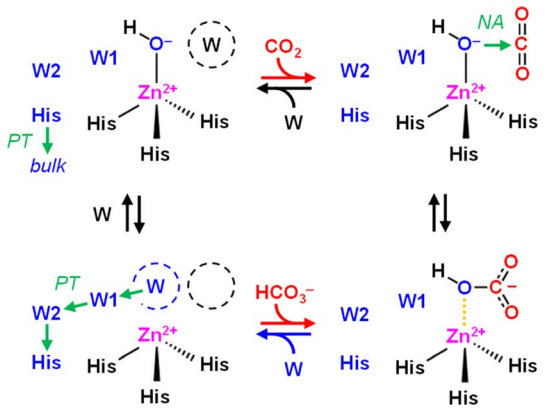

Scheme 1 Mechanism of CO_2 hydration in carbonic anhydrase. Top row, left to right: CO_2 enters the active site and replaces a water molecule (W, black) near the zinc cation (Zn^{2+}). In the next step, CO_2 is converted to HCO_3^- upon a nucleophilic attack (NA) of the zinc-bound hydroxide (Zn^{2+}–OH^-). Bottom row, right to left: HCO_3^- is replaced by another water molecule (W, blue), the latter which is activated to OH^- upon proton transfer (PT) *via* oriented water molecules W1 and W2 and a conserved histidine (His, blue). In the last step, this histidine changes its orientation to release the proton into bulk solvent, and water re-binds (W, black) near the active site.

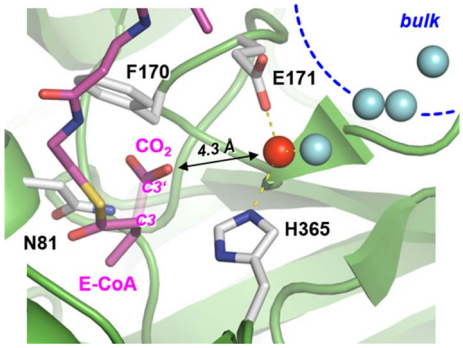

Fig. 1 Active site of crotonyl CoA carboxylase/reductase. Crystal structure of *Ks*Ccr in complex with reaction product ethylmalonyl coenzyme A, E-CoA (PDB ID 6OWE). The bond between C3 and C3′ of E-CoA is drawn translucent to emphasize the CO_2 binding site. *Ks*Ccr active site residues F170 and N81 interact with E-CoA while H365 and E171 coordinate a 'bridging' water molecule, μW (red sphere, distance to H365 and E171 each 2.8 Å). A local water cluster connects the active site with bulk solvent (blue spheres, shortest distance to μW 2.9 Å).

binding is achieved through four amino acid residues and one conserved water molecule that is coordinated by an aspartate E171 and a histidine H365 (μW).[12]

All molecular species involved in the above described CO_2-conversions (H_2O, CO_2, HCO_3^-) show characteristic absorbance between 4000–1000 cm^{-1}, which makes them available to Fourier-transform infrared (FTIR) spectroscopy.[13–16] In a protein sample, however, these signals are overlaid by the intense absorbance of bulk water and the amide bands of the protein backbone.[17] This limitation can be overcome by FTIR difference spectroscopy, which provides the means to distinguish between protein sample background signals and the signature of a given reaction upon a specific trigger.[18] We developed a FTIR difference spectroscopy-based setup in which catalysis can be triggered *via* the gas phase.[19] Compared to the conventional transmission configuration a protein film is formed on top of the silicon crystal of an attenuated total reflection (ATR) optical cell,[20] which makes the protein amendable to changes in the gas phase, *e.g.*, by switching from a inert carrier gas (100% N_2 or Ar, defining the background signal) to a 'reactive' gas mixture (see ESI† for further details). This specific design allows studying the reaction of CO_2-converting enzymes providing the substrate (*i.e.*, CO_2) *in situ* and thus the reaction trigger for these enzymes.[19]

Here, we applied *in situ* ATR FTIR spectroscopy to study the interaction of *Ks*Ccr with CO_2. Our results show that the active site of *Ks*Ccr does not only bind CO_2 but surprisingly possesses a so-far unknown, intrinsic CA-like activity, which enables the enzyme to catalyze the reversible interconversion of CO_2, H_2O, and HCO_3^-. Studying the reaction in absence or presence of substrates or inhibitors with wild-type and five active site variants, we identified key residues for the observed CA-like activity including a cluster of strongly hydrogen-bonded, 'local' water molecules. Moreover, computer simulations suggest that conformational dynamics and substrate binding in *Ks*Ccr modulate CO_2 binding at the active site. Combining experiment and simulation, we propose a mechanism for the CA-like activity of *Ks*Ccr that involves an 'activated' water molecule, which is essential for CO_2-binding during the CO_2-fixation reaction of *Ks*Ccr but also serves as nucleophilic OH^- anion in the enzyme's CA-like reaction.

Results and discussion

Infrared signatures of anhydrase activity

First, we pipetted 1 µl *Ks*Ccr solution (200 µM protein in 25 mM Tris/HCl pH 7.5) on the ATR crystal of the FTIR spectrometer and monitored water evaporation under dry N_2 gas *in situ*. Once sufficiently concentrated, we rehydrated the protein film under a stream of aerosol that was created by sending dry N_2 gas (3 L min^{-1}) through a wash bottle containing a dilute Tris/HCl buffer solution (1 mM, pH 7.5). Then, we added 10% CO_2 to the N_2 carrier gas for 50–100 s and recorded data to calculate a series of time-resolved *in situ* ATR FTIR difference spectra that result from the interaction of *Ks*Ccr with CO_2 (Fig. S1†). In reference experiments with pure water and buffer solution, 25 mM Tris/HCl (pH 8) was found to be sufficiently concentrated preventing acidification in the presence of 10% CO_2 (Fig. S2†).

Fig. 2A depicts a 'CO_2–N_2' FTIR difference spectrum recorded 25 s after addition of 10% CO_2. The positive band at 2341 cm^{-1} corresponds to CO_2 in solution.[13] Further positive bands were observed at 1618 cm^{-1}, 1358 cm^{-1}, and 1298 cm^{-1}, the latter as a shoulder. These bands are assigned to bicarbonate in solution,[14–16] *i.e.*, the asymmetric and symmetric stretching modes of CO_2 (ν_2, ν_3) and the HCO_3^- bending mode (ν_4). A broad negative band at 3000 cm^{-1} appeared in an energy regime corresponding to a strongly hydrogen-bonded network of 'local' water molecules,[21–23] indicating that water is consumed during bicarbonate formation.

Open Access Article. Published on 29 February 2024. Downloaded on 2/8/2026 11:43:49 AM.
This article is licensed under a Creative Commons Attribution 3.0 Unported Licence.

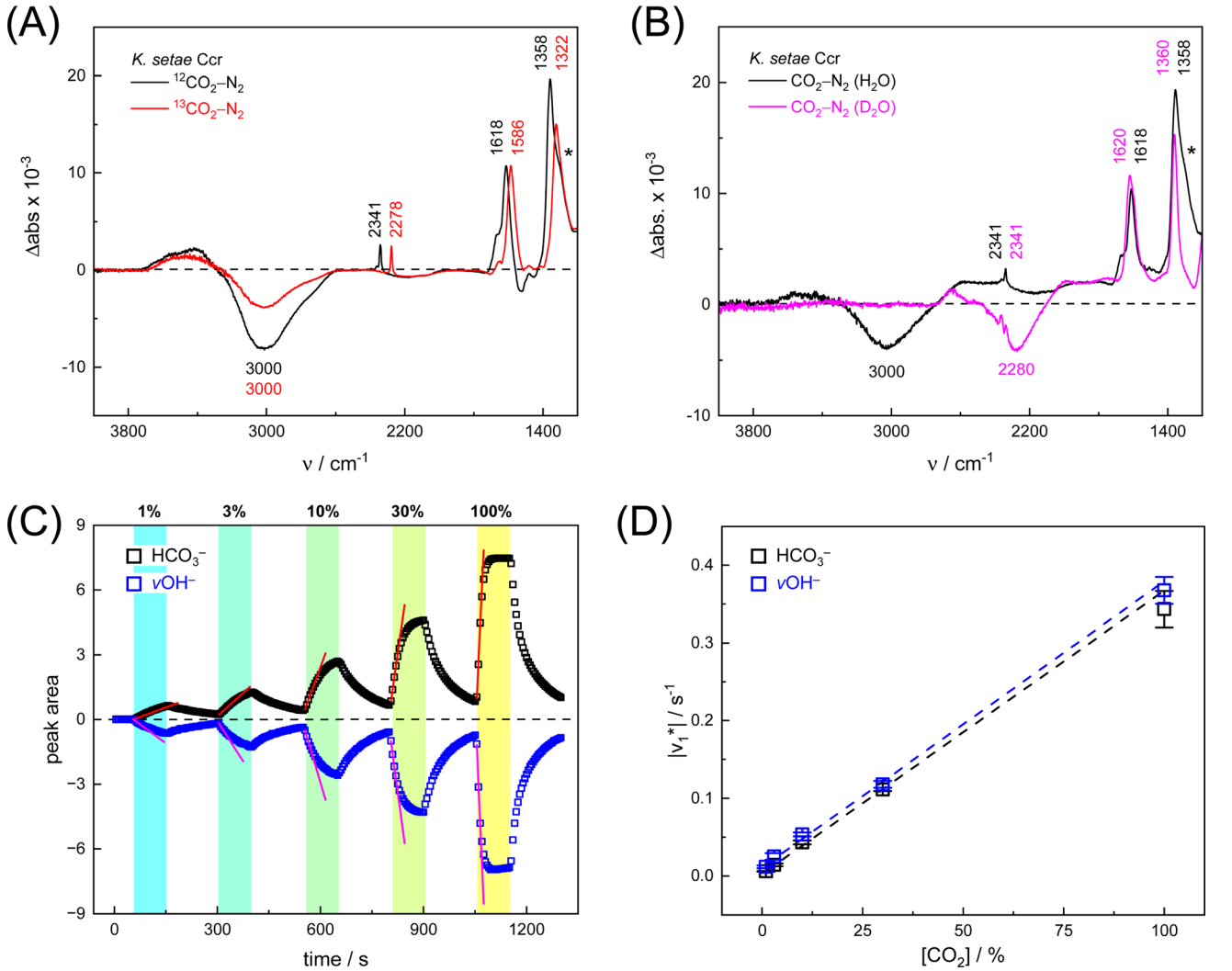

Fig. 2 Infrared characterization of the reaction of *Ks*Ccr with CO_2. (A) 'CO_2–N_2' ATR FTIR difference spectra for the reaction with $^{12}CO_2$ (black) or $^{13}CO_2$ (red). Positive signals are assigned to CO_2 (2341 or 2278 cm^{-1}) and HCO_3^-. The COH vibration (ν_4) appears as a shoulder at 1298 cm^{-1} (*). (B) 'CO_2–N_2' ATR FTIR difference spectra in the presence of H_2O (black) or D_2O (magenta). The broad negative bands are assigned to 'local' water with νOH^- = 3000 cm^{-1} and νOH^- = 2280 cm^{-1}. (C) Evolution of the bands assigned to HCO_3^- (black) and νOH^- (blue) over time in the presence of 1–100% CO_2 or 100% N_2. Red lines represent linear fits of the first three data points after gas exchange to calculate the initial reaction velocity ν_1^*. (D) Plot of the apparent reaction velocity $|\nu_1^*|$ of the initial HCO_3^- formation (black) or initial water consumption (blue) in the CO_2 hydration reaction.

To confirm assignment of the observed bands, we investigated potential isotope effects. Adding $^{13}CO_2$ gas instead of CO_2 resulted in a specific down-shift of the CO_2 band to 2278 cm^{-1} (Δ63), as well as the ν_2 and ν_3 bands of HCO_3^- to 1586 cm^{-1} and 1322 cm^{-1} (Δ32 and Δ36, respectively). The isotope effect on the band at 1258 cm^{-1} was rather minor while the broad negative band at 3000 cm^{-1} was not affected by $^{13}CO_2$, which is in line with our assignments of CO_2/HCO_3^- and 'local' water. We also investigated the influence of solvent isotope effects by exchanging the hydrated *Ks*Ccr protein film from H_2O to D_2O (Fig. 2B). In the presence of D_2O, we observed a large down-shift of the negative band from 3000 cm^{-1} to 2280 cm^{-1} (Δ720) supporting our assignment of the water cluster. While the H/D exchange only had an insignificant effect on the ν_2 and ν_3 bands, the shoulder at 1298 cm^{-1} seemed to disappear in the deuterated sample. This is due to a ~300 cm^{-1} down-shift that moves the signal out of the detection window of our FTIR setup and additionally confirms the COH (ν_4) assignment.[15]

Next, we studied the kinetics of the reaction between *Ks*Ccr and CO_2. The difference spectra were simulated with contributions from CO_2, H_2O, and HCO_3^- and corrected for unspecific changes (Fig. S3†). The resulting 'peak area' for each reactant was plotted against time. Fig. 2C shows the changes of HCO_3^- (given by the sum of ν_2, ν_3, and ν_4) and 'local' water (νOH^-) in *Ks*Ccr upon reaction with CO_2. We titrated the enzyme in five consecutive steps changing the gas atmosphere to a continuous partial pressure of 1, 3, 10, 30, and 100% CO_2 followed by exposure to 100% N_2 after each CO_2 step. Qualitatively, these data demonstrate that the intensity of the HCO_3^- and water bands are proportional to the CO_2 concentration in

© 2024 The Author(s). Published by the Royal Society of Chemistry

Open Access Article. Published on 29 February 2024. Downloaded on 2/8/2026 11:43:49 AM.
This article is licensed under a Creative Commons Attribution 3.0 Unported Licence.

the atmosphere and that the CO_2/HCO_3^- conversion is reversible (eqn (1)). The initial velocity of CO_2 hydration (ν_1^*) was estimated by linear regression based on the first three data points after changing the atmosphere from N_2 to CO_2 for each step. We assume that the reaction velocity is not significantly affected by the back reaction due to the small build-up of HCO_3^- within the first 15 s. A similar approach was chosen to quantify the initial velocity of HCO_3^- dehydration (ν_{-1}^*) initiated by removing CO_2 from the gas atmosphere (Fig. S4†). The data yielded apparent reaction velocities ν_1^* and ν_{-1}^* that are specific for our experimental approach. Earlier, we explored how the humidity of concentrated protein films influences the velocity of substrate diffusion[24,25] and its overall elastic properties.[26] Now, we show that corresponding observations are made with *Ks*Ccr: when the humidity was reduced from 75% to 35% (determined *via* the OH stretching vibrations of H_2O, see Fig. S3†) the velocity of CO_2 hydration decreased accordingly (Fig. S5†). Although the spectroscopically measured velocities are lower than in solution assays[27] our data facilitates a quantitatively significant comparison between samples under tightly controlled steady-state conditions. To demonstrate the catalytic activity of *Ks*Ccr in solution, we performed the 'colorimetric' analysis of CO_2 hydration as pioneered by Wilbur and Anderson.[28] Here, the injection of a defined amount of CO_2-saturated buffer induces an acidification (eqn (1)), which leads to a bleach of a strong absorbance band of bromothymol blue that can be followed over time by UV/vis spectroscopy. Our data in Fig. S6† demonstrate that CO_2 hydration in aqueous solution is much slower than in the presence of *Ks*Ccr or β-type carbonic anhydrase from *E. coli* (*Ec*CA) confirming the observed anhydrase activity of *Ks*Ccr.[29]

Fig. 2D shows how the calculated reaction velocities for HCO_3^- formation and water consumption (given in absolute values $|\nu_1^*|$ to visually aid the comparison) depend linearly on the CO_2 concentration. The experimental variation has been determined in repetitions of five (Fig. S7†). This confirms the proposed reaction model of pseudo-first order kinetics for enzymatic CO_2 hydration in aqueous solution[30] and highlights the quantitative connection between CO_2, HCO_3^-, and water in the active site. Fig. S8† depicts a quantification of HCO_3^- based on Na_2CO_3 reference samples and an analysis of the exponential correlation between CO_2 partial pressure and HCO_3^- concentration in the protein film. This facilitates the analysis of the initial velocity of the back reaction (ν_{-1}^*) as a function of bicarbonate concentration. The data in Fig. S4† suggest a higher reaction order and overall slower kinetics. We speculate that the apolar active site of *Ks*Ccr (Fig. 1) may slow down HCO_3^- binding, which would impede the back reaction.

To verify and benchmark the CO_2/HCO_3^- conversion by *Ks*Ccr, we repeated the experiments with carbonic anhydrase *Ec*CA at conditions comparable to the experiments with *Ks*Ccr. The 'CO_2–N_2' FTIR spectrum for *Ec*CA after 25 s in the presence of 10% CO_2 (Fig. 3A) is strikingly similar to the one observed for *Ks*Ccr (Fig. 2B) including the positive features for CO_2 and HCO_3^-, as well as the negative water band at 3050 cm^{-1} (2300 cm^{-1} in D_2O). However, Fig. 3B shows that *Ec*CA catalyses the CO_2/HCO_3^-conversion nearly four times faster than *Ks*Ccr

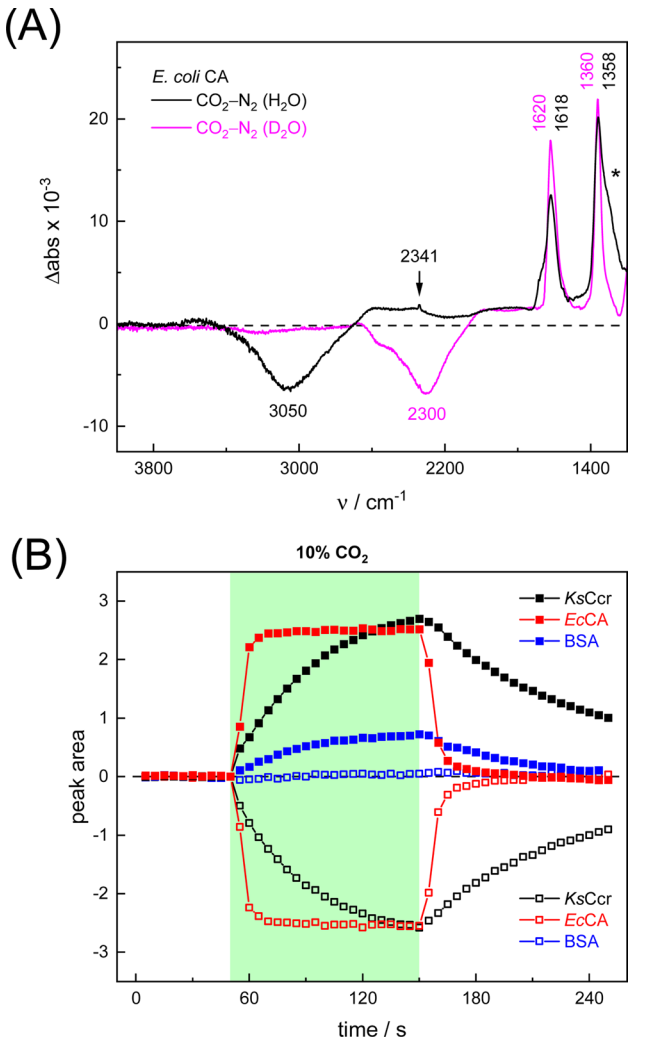

Fig. 3 Infrared characterization of the reaction of *Ec*CA with CO_2. (A) 'CO_2–N_2' ATR FTIR difference spectra in the presence of H_2O (black) or D_2O (magenta). These data show that *Ec*CA and *Ks*Ccr (Fig. 2) react very similar with CO_2. (B) Plotting the evolution of spectral traces for HCO_3^- (closed symbols) and νOH^- (open symbols) against time, the superior reaction velocity of *Ec*CA (red) over *Ks*Ccr (black) and BSA background (blue) becomes evident.

($\nu_1^* \approx 0.22$ s^{-1} and 0.06 s^{-1}, respectively). The superior activity of *Ec*CA is observed in solution as well (Fig. S6†). For comparison unspecific CO_2 conversion by bovine serum albumin (BSA, $\nu_1^* \approx 0.016$ s^{-1}) is plotted in Fig. 3B. Note the lack of a negative band at 3000 cm^{-1}

The CO_2 conversion kinetics of *Ks*Ccr in Fig. 2 are in the range of uncatalyzed CO_2 hydration in solution (Fig. S6†). Therefore, we probed background CO_2 conversion in (i) water, (ii) buffer, and (iii) BSA as a generic biological crowder.[31] No significant HCO_3^- formation was observed with pure water, presumably due to the acidification in unbuffered solution (Fig. S2†). When recording 'CO_2–N_2' difference spectra on a drop of Tris/HCl buffer (2 μl, 25 mM, pH 8) approximately 10% HCO_3^- formation was observed within the same time frame as in the *Ks*Ccr experiments (Fig. S2†) although much more CO_2 is dissolved in the drop compared to *Ks*Ccr or *Ec*CA (Fig. S9†). As

© 2024 The Author(s). Published by the Royal Society of Chemistry

Open Access Article. Published on 29 February 2024. Downloaded on 2/8/2026 11:43:49 AM.
This article is licensed under a Creative Commons Attribution 3.0 Unported Licence.

argued above, data based on liquid sample cannot be compared directly, therefore we formed a BSA protein film to probe uncatalyzed CO_2 hydration under conditions comparable to the experiments with *Ks*Ccr or *Ec*CA. At pH 7–8, BSA shows up to 30% of the bicarbonate formation activity observed with *Ks*Ccr and a HCO_3^-/CO_2 ratio similar to *Ks*Ccr or *Ec*CA. However, the unique water feature of *Ks*Ccr and *Ec*CA is shifted to 3320 cm^{-1}, indicative of uncatalyzed CO_2 hydration from bulk water (Fig. S9†). Accordingly, when the BSA solution was adjusted to pH values between 5–9, the observed HCO_3^- formation resembles the pH profile of the CO_2/HCO_3^- couple in the absence of enzyme. Note that this is not the case for *Ks*Ccr: in the same pH range, this enzyme shows largely unchanged CO_2 hydration activity (Fig. S9†). Overall, these controls demonstrated that *Ks*Ccr possesses a CA-like activity similar to the reaction of 'true' CAs.

Substrate binding and hydrophilic residues influence anhydrase activity

In the next step, we investigated the CO_2/HCO_3^- conversion activity of *Ks*Ccr in the presence of NADPH, $NADP^+$, native substrate crotonyl-coenzyme A (C-CoA), and side product butyryl-coenzyme A (B-CoA).[9–11] We tested six different combinations: (i) *Ks*Ccr only, (ii) *Ks*Ccr + 10 mM $NADP^+$, (iii) *Ks*Ccr + 10 mM NADPH, (iv) *Ks*Ccr + 10 mM NADPH + 1 mM C-CoA, (v) *Ks*Ccr + 1 mM C-CoA, and (vi) *Ks*Ccr + 1 mM B-CoA. Fig. 4A shows the HCO_3^- peak area observed after 60 s in the FTIR difference experiments (*i.e.*, upon saturation of the signals, see Fig. S9†), normalized to wild-type *Ks*Ccr, which defines '100%' bicarbonate formation. The experimental variation has been determined in repetitions of five (Fig. S7†). In these experiments, neither NADPH nor $NADP^+$ affected bicarbonate formation, while the presence of C-CoA or B-CoA decreased band intensity down to 33% and 17%, respectively. Based on our reference experiments (Fig. S9†), we note that about 30% CO_2 hydration can be considered as background activity, which is indicated by the dashed line in Fig. 4A. These data suggest that HCO_3^- formation and carboxylation are mutually exclusive indicating that the CO_2/HCO_3^- conversion occurs only at the substrate-free active site of *Ks*Ccr. We speculate that the superior inhibition activity of B-CoA is related to the structural flexibility of this catalytic side product, which has been shown to fit the active site of *Ks*Ccr smoothly.[32] These properties might affect unspecific binding site as well pushing the activity below the threshold.

We have shown previously that four amino acids play a key role in CO_2 binding at the active site of *Ks*Ccr: histidine H365, glutamate E171, asparagine N81, and phenylalanine F170.[12] H365 and E171 are involved in coordinating a conserved water molecule in bridging position (μW), which is in hydrogen-bonding contact with water molecules that connect the active site with bulk water (Fig. 1). Asparagine N81 orients CO_2 in the active site for the carboxylation reaction, and F170 shields the pocket from water.

To understand the molecular basis of CO_2/HCO_3^- conversion in *Ks*Ccr, we tested five active site variants. Qualitatively,

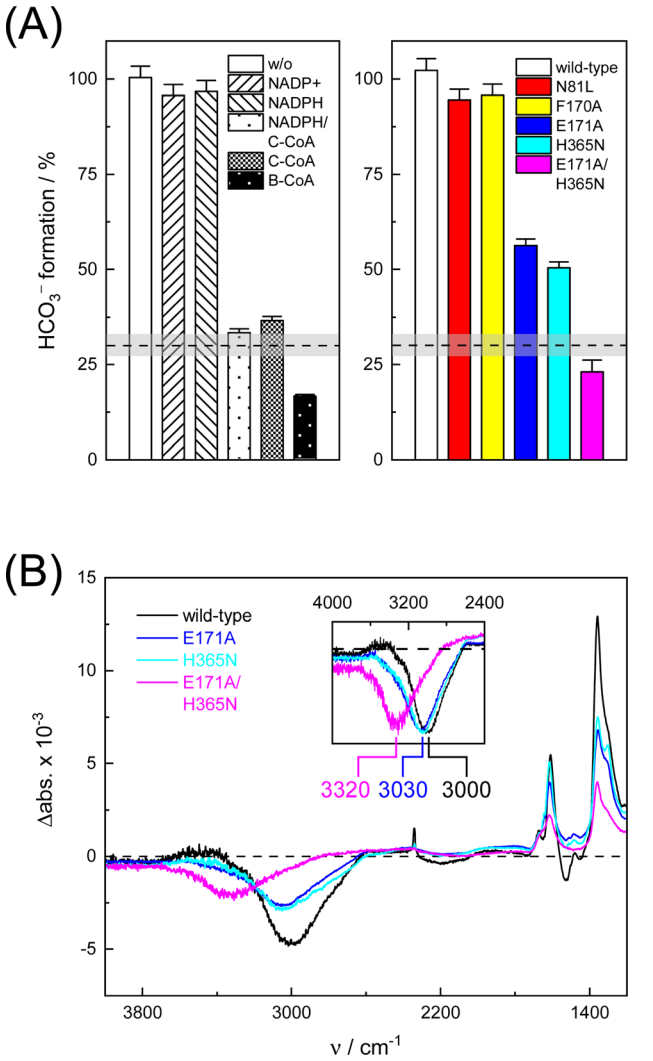

Fig. 4 Bicarbonate formation activity of wild-type *Ks*Ccr and variants. (A) The HCO_3^- peak area after 60 s in the presence of 10% CO_2 is set to 100% for wild-type *Ks*Ccr and compared for different conditions (left panel) and active site variants (right panel) as annotated in the bar plot. About 30% CO_2 hydration can be considered as unspecific background activity, which is indicated by the dashed line. (B) 'CO_2–N_2' FTIR difference spectra after 60 s highlight quantitative differences (*i.e.*, the intensity of the bicarbonate bands) and qualitative differences between wild-type *Ks*Ccr and variants: the inset shows an up-shift of the water band (scaled), most clearly visible for *Ks*Ccr double variant E171A/H365N (magenta).

the 'CO_2–N_2' FTIR difference spectra of single point mutants N81L, F170A, E171A, and H365N were similar to wild-type *Ks*Ccr. However, while N81L and F170A showed full conversion, bicarbonate formation of variants E171A and H365N was reduced by *ca.* 50% (Fig. 4A). Compared to H365N variant E171A showed slightly slower bicarbonate formation. In the *Ks*Ccr E171A/H365N double mutant both conversion and reaction velocity were found to be reduced even further (Fig. S10†). Fig. 4B highlights an interesting detail in the difference spectra of wild-type *Ks*Ccr, E171A, H365N, and E171A/H365N: the water band shifts from 3000 cm^{-1} to 3030 cm^{-1} in the single point mutants and all the way down to 3320 cm^{-1} in the double

© 2024 The Author(s). Published by the Royal Society of Chemistry

Open Access Article. Published on 29 February 2024. Downloaded on 2/8/2026 11:43:49 AM. This article is licensed under a Creative Commons Attribution 3.0 Unported Licence.

mutant. This indicates that *Ks*Ccr E171A/H365N has lost its CA-like activity and exhibits only unspecific CO_2 hydration much like BSA that showed a similar 'CO_2–N_2' FTIR difference spectrum (Fig. S9†) and in agreement with the reduced CO_2 hydration activity reported in Fig. 4A. In summary, these experiments suggest that the CA-like activity depends on the active site of *Ks*Ccr, and likely involves E171 and H365.

Computer simulations reveal conformation-dependent CO_2 binding and explain substrate inhibition

To rationalize the observed inhibition of CA-like activity through substrate binding, we performed atomistic MD simulations in the presence of CO_2 using the X-ray crystal structure of *Ks*Ccr that binds both NADPH and side product B-CoA (ternary complex, PDB ID 6NA4).[32] Note that the enzyme is a tetramer that shows half-site reactivity, *i.e.*, exists as dimer of open and closed subunits (colored orange and green in Fig. 5). Compared to the open subunits the closed subunits contain the substrate and represent the catalytically active sites in the ternary complex. For our simulations, we replaced B-CoA by C-CoA and defined a specific volume box (Fig. 5) to calculate the CO_2 binding free energy in the open and closed subunit. Notably, active site residues H365 and E171, which we associate with CA-like activity, adopted different geometries in the open and closed conformations. Compared to the open subunit, the distance between E171 and H365 was 3 Å shorter in the closed subunit and the conserved water molecule μW was hydrogen-bonded between the two residues (Fig. 5). Additionally, we studied the X-ray structure without substrate (binary complex, PDB ID 6NA4) that presents similar geometries of both residues in the closed and open subunits.[32]

We presume that H365 can act as base in its neutral, monoprotonated state initiating proton abstraction from μW and thus forming the hydroxyl ion for subsequent CO_2 hydration. To determine the protonation state of H365 in different subunits of the binary and ternary complexes, we calculated the pK_a shift (Table S1†).[33] For the open active site, the pK_a shift is negative ($\Delta pK_a = -0.9 \pm 0.1$) indicating that H365 rather adopts a monoprotonated state. For the closed active site without substrate (binary complex), we also obtained a negative shift ($\Delta pK_a = -0.6 \pm 0.1$) while the p$K_a$ shift was positive in the presence of the substrate ($\Delta pK_a = +1.2 \pm 0.1$), likely because of favorable interactions of the H365 with the negatively charged phosphate groups of C-CoA. Thus, H365 is monoprotonated in the empty, closed active site and capable of initiating proton abstraction from μW. In the presence of substrate H365 most likely changes its protonation state, thus suppressing CA activity.

In addition, CO_2 binding to the active site plays an important role. To understand the influence of conformational changes and presence of the substrate on CO_2, we carried out extensive MD simulations. From the ratio of local CO_2 concentration in the active site volume (black box in Fig. 5) and the concentration in the bulk we calculated the CO_2 binding free energy to the active site volume for the open and closed subunits of the binary and ternary complexes of *Ks*Ccr ($\Delta G_{bind} = -k_B T \ln\left(\frac{c_{act.\ site}}{c_{bulk}}\right)$, see ESI†). Our calculations show that ΔG_{bind} of the closed subunit with substrate (ternary complex) is positive whereas the closed subunit in the binary complex without substrate presents the highest CO_2 affinity which makes it more than two times more probable to find a CO_2 molecule in the active site than in the bulk (Fig. 6A). The open subunit in the ternary complex also shows a significantly increased CO_2 affinity but the distance between E171 and H365 is larger in the open active site, and no μW molecule is observed suggesting a diminished catalytic activity. We then addressed the binding sites of CO_2 in the closed active site without substrate where the affinity is highest. The binding sites connect active site interior and solvent, and the most buried ones are very close to H365, water molecule μW,

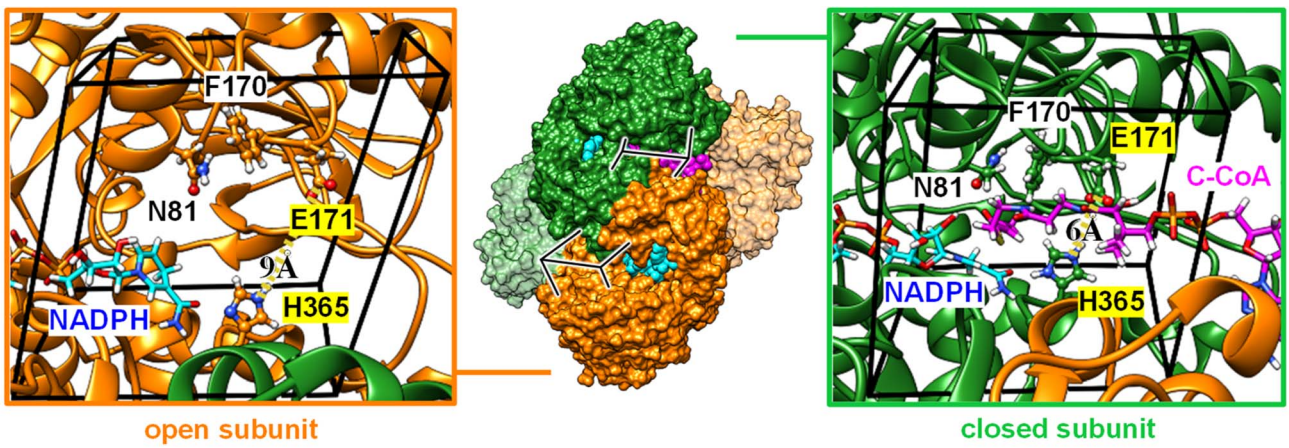

Fig. 5 Computational model. Crystal structure of *Ks*Ccr (PDB ID 6NA4) in a dimer-of-dimers configuration with open subunits (orange, left panel) and closed subunits (green, right panel). A close-up to the active site for the open and closed subunit shows residues N81, F170, E171, and H365. Note that the E171/H365 distance shrinks from 9 Å to 6 Å in the closed subunit. A black box encloses the volume of the active site used to analyze the local CO_2 concentration. NADPH is shown in cyan sticks, C-CoA is shown in magenta sticks. The later is exclusively found in the closed subunit (green, right panel).

© 2024 The Author(s). Published by the Royal Society of Chemistry

Open Access Article. Published on 29 February 2024. Downloaded on 2/8/2026 11:43:49 AM. This article is licensed under a Creative Commons Attribution 3.0 Unported Licence.

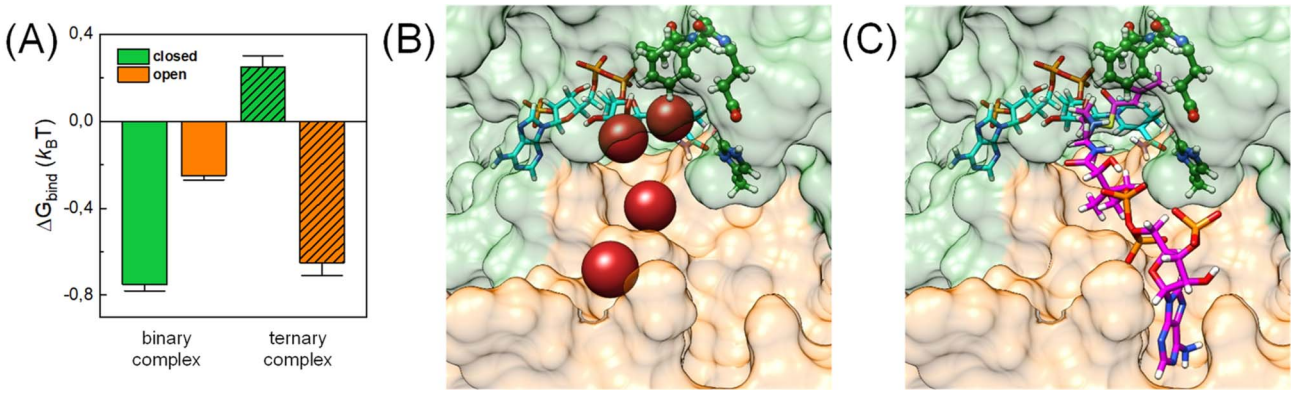

Fig. 6 CO_2 binding in the active site of *Ks*Ccr. (A) Binding free energy (k_BT) of CO_2 in the closed and open subunit of the binary complex with NADPH and the ternary complex with NADPH and C-CoA from MD simulations. (B) Most probable binding sites of CO_2 in the closed active site of the binary complex (PDB ID 6NA6) represented as red spheres. (C) Representative snapshot of the ternary complex (PDB ID 6NA4), in which the substrate occupies the position of the CO_2 binding sites. NADPH is shown in cyan, C-CoA is shown in magenta, and key residues are shown in green sticks.

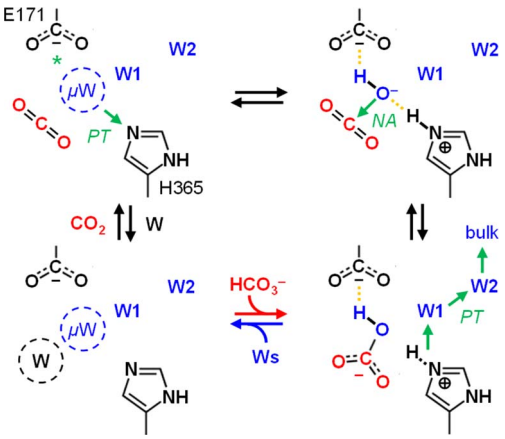

Scheme 2 Proposed reaction mechanism. Top row, left to right: interstitial water μW is deprotonated *via* H365 (*or E171 in the H365N variant) when the system adopts the closed state. The resulting μOH^- species is stabilized by hydrogen bonds (dashed lines) and attacks a bound CO_2 molecule to form bicarbonate HCO_3^-. Bottom row, right to left: when the system adopts the open state, HCO_3^- leaves the active site and H365 releases a proton toward bulk solvent. Influx of water and CO_2 primes *Ks*Ccr for another round of anhydrase activity.

and E171 (Fig. 6B). Notably, the substrate in the ternary complex occupies the same positions as the CO_2 binding sites (Fig. 6C).

In summary, our computer simulations show that the binary complex has a higher CO_2 binding affinity compared to the ternary complex. The CO_2 binding sites in the closed active site are next to H365 and the conserved water molecule μW, so that the monoprotonated form of H365 will be able to abstract a proton from μW to form the nucleophilic hydroxyl ion. The absence of NADPH or $NADP^+$ is not expected to affect CO_2 binding or H365 protonation because the coenzyme does not bind directly to the substrate binding site.[32] In contrast, the presence of C-CoA or B-CoA in the ternary complex increases the pK_a of the putative proton acceptor H365 thereby eliminating its ability to activate μW water by proton transfer, and simultaneously diminishes CO_2 binding. This can explain the experimentally observed reduction of CA-like activity and is in line with the fact that the active enzyme ternary complex promotes CO_2 fixation,[32] and not CO_2 hydration.

Conclusions

In this study, we applied *in situ* ATR FTIR difference spectroscopy and computer simulations to investigate and understand the interaction of crotonyl-CoA carboxylase/reductase (*Ks*Ccr) with CO_2. Our results show that *Ks*Ccr possesses a carbonic anhydrase-like activity, *i.e.*, the interconversion of CO_2 and HCO_3^- with water. This reaction is strongly suppressed in the presence of C-CoA, the natural substrate of *Ks*Ccr. Extensive MD simulations revealed how C-CoA suppresses CO_2 binding and identified H365 as putative proton acceptor during CO_2 hydration. Compared to wild-type *Ks*Ccr variant H365N indeed showed about 50% reduced anhydrase activity, similar to variant E171A. Our pK_a calculations rationalize how either H365 or E171 can serve as 'base' in the CO_2 hydration reaction explaining the relatively large anhydrase activity of the single-residue variants. In contrast, only slow and unspecific CO_2 hydration is observed with double variant E171A/H365N. In wild-type *Ks*Ccr, H365 and E171 form a hydrogen-bonding complex through an interstitial, bridging water molecule (μW). The latter is in contact with a chain of water molecules that facilitate contact with bulk water. Upon CO_2 hydration our FTIR data reveal the loss of a broad band at 3000 cm^{-1} (2280 cm^{-1} in D_2O), which we assign to a strongly hydrogen-bonded water cluster, most likely including μW.

Notably, we also observed very similar spectra for *Ec*CA, which we used as a reference to validate the experimental setup and confirm our interpretation of *Ks*Ccr's CA-like activity. *Ec*CA coordinates a zinc cofactor that catalyses the deprotonation of a bound water molecule to a hydroxide ligand (Zn^{2+}–OH^-) promoted by a nearby histidine base (Scheme 1). CO_2 reacts with the ligand to HCO_3^-, which is clearly observed in our FTIR difference spectra as a positive contribution. In the following HCO_3^- leaves the active site and is replaced by another water

© 2024 The Author(s). Published by the Royal Society of Chemistry

Open Access Article. Published on 29 February 2024. Downloaded on 2/8/2026 11:43:49 AM. This article is licensed under a Creative Commons Attribution 3.0 Unported Licence.

molecule. Binding of water 're-activates' the cofactor, resulting in a broad negative band in our FTIR difference spectra, similar to what we have observed with *Ks*Ccr. Reported here for the first time, these results establish a unique spectral signature of CA activity, *i.e.*, the IR bands of bicarbonate and a strongly-hydrogen bonded cluster of 'local' water.

The role and importance of a metal ion in CA has been discussed intensively.[8] However, in 2021 Hirakawa *et al.* reported metal-free CAs in cyanobacteria and microalgae that appear to catalyse CO_2 hydration in a purely organic environment.[34] These observations are in line with our experiments on *Ks*Ccr that also suggest metal-independent CA-like activity. Based on our combined experimental and theoretical investigation of CO_2 hydration in *Ks*Ccr, we propose a mechanism related to carbonic anhydrase (Scheme 2): (i) Once the enzyme adopts the closed state, μW is deprotonated to a bridging hydroxide, μOH^-, with the neutral H365 residue serving as base (our pK_a calculations suggest that E171 may serve as base in H365 variants, see Table S1†). (ii) The carboxylate side chain of E171 accepts a hydrogen bond from μOH^-, which itself is stabilized *via* a hydrogen bond from the imidazole side chain of protonated H365. When CO_2 is present in the active site μOH^- will form HCO_3^- *via* a nucleophilic attack (NA, the reaction may involve additional water species, see Fig. S11†). (iii) Bicarbonate leaves the active site – potentially triggered by a transition from the closed to the open state – and deprotonation of H365 toward bulk solvent. We speculate that the protonated imidazolium cation is not stable in the absence of an interstitial water species. (iv) This transient opening of the hydrogen-bonding complex will allow intake of water and CO_2 and prime the system for a new round of CO_2 hydration.

Summing up, *in situ* ATR FTIR difference spectroscopy allowed investigating the interaction of different enzymes with CO_2, providing a simple yet powerful approach to directly identify CA activity for a given biological sample. Moreover, our method is also suited to identify and characterize water clusters and will serve as an important tool to analyze CO_2 hydration in biocatalysis,[35–38] homogenous or heterogeneous catalysts,[39–41] and (de-)hydration reactions in general.[42,43]

Data availability

Data are available from the authors upon reasonable request.

Author contributions

M. Tinzl, G. Stoffel, and H. Westedt produced and prepared the enzymes. A. Gomez performed the molecular dynamics simulations and pK_a calculations. S. T. Stripp designed and performed the spectroscopy experiments. H. Grubmüller, T. J. Erb, E. Vöhringer-Martinez and S. T. Stripp discussed the data. E. Vöhringer-Martinez designed the computer simulations. E. Vöhringer-Martinez and S. T. Stripp wrote the manuscript.

Conflicts of interest

There are no conflicts to declare.

Acknowledgements

The authors acknowledge help from Mariafrancesca Greca and Federico Baserga at Freie Universität Berlin in buffer exchange experiments and UV/vis spectroscopy. EVM and AG are thankful for financial support provided by the Max-Planck Society (MPS) through the CONICYT Program of Int. Cooperation with the Max Planck for Terrestrial Microbiology in Marburg (MPG190003) and PhD scholarship "Doctorado Nacional" (21190262) provided by ANID. MT is thankful for a Postdoctoral Fellowship from the Swiss National Science Foundation (P500PB 203136). MT and TJE received support from the MPS the European Research Council (ERC 637675 'SYBORG'). STS thanks funding by the Deutsche Forschungsgemeinschaft DFG (priority program 1927 "Iron-Sulfur for Life", STR1554/5-1).

References

1 S. Bierbaumer, M. Nattermann, L. Schulz, R. Zschoche, T. J. Erb, C. K. Winkler, M. Tinzl and S. M. Glueck, *Chem. Rev.*, 2023, **123**, 5702–5754.
2 R. Wolfenden, *Chem. Rev.*, 2006, **106**, 3379–3396.
3 R. J. DiMario, M. C. Machingura, G. L. Waldrop and J. V. Moroney, *Plant Sci.*, 2018, **268**, 11–17.
4 D. W. Christianson and C. A. Fierke, *Acc. Chem. Res.*, 1996, **29**, 331–339.
5 D. N. Silverman and R. McKenna, *Acc. Chem. Res.*, 2007, **40**, 669–675.
6 V. M. Krishnamurthy, G. K. Kaufman, A. R. Urbach, I. Gitlin, K. L. Gudiksen, D. B. Weibel and G. M. Whitesides, *Chem. Rev.*, 2008, **108**, 946–1051.
7 C. T. Supuran, *Biochem. J.*, 2016, **473**, 2023–2032.
8 J. K. Kim, C. Lee, S. W. Lim, A. Adhikari, J. T. Andring, R. McKenna, C. M. Ghim and C. U. Kim, *Nat. Commun.*, 2020, **11**, 1–10.
9 T. J. Erb, I. A. Berg, V. Brecht, M. Müller, G. Fuchs and B. E. Alber, *Proc. Natl. Acad. Sci. U. S. A.*, 2007, **104**, 10631–10636.
10 T. J. Erb, V. Brecht, G. Fuchs, M. Müller and B. E. Alber, *Proc. Natl. Acad. Sci. U. S. A.*, 2009, **106**, 8871–8876.
11 R. G. Rosenthal, M.-O. Ebert, P. Kiefer, D. M. Peter, J. A. Vorholt and T. J. Erb, *Nat. Chem. Biol.*, 2014, **10**, 50–55.
12 G. M. M. Stoffel, D. A. Saez, H. DeMirci, B. Vögeli, Y. Rao, J. Zarzycki, Y. Yoshikuni, S. Wakatsuki, E. Vöhringer-Martinez and T. J. Erb, *Proc. Natl. Acad. Sci. U. S. A.*, 2019, **116**, 13964–13969.
13 M. Falk and A. G. Miller, *Vib. Spectrosc.*, 1992, **4**, 105–108.
14 A. R. Davis and B. G. Oliver, *J. Solution Chem.*, 1972, **1**, 329–339.
15 W. W. Rudolph, D. Fischer and G. Irmer, *Appl. Spectrosc.*, 2006, **60**, 130–144.
16 E. Garand, T. Wende, D. J. Goebbert, R. Bergmann, G. Meijer, D. M. Neumark and K. R. Asmis, *J. Am. Chem. Soc.*, 2010, **132**, 849–856.
17 A. Barth, *Biochim. Biophys. Acta, Bioenerg.*, 2007, **1767**, 1073–1101.
18 V. A. Lórenz-Fonfria, *Chem. Rev.*, 2020, **120**, 3466–3576.
19 S. T. Stripp, *ACS Catal.*, 2021, **11**, 7845–7862.

© 2024 The Author(s). Published by the Royal Society of Chemistry

Open Access Article. Published on 29 February 2024. Downloaded on 2/8/2026 11:43:49 AM.
This article is licensed under a Creative Commons Attribution 3.0 Unported Licence.

20 J. Fahrenfort, *Spectrochim. Acta*, 1961, **17**, 698–709.
21 F. N. Keutsch and R. J. Saykally, *Proc. Natl. Acad. Sci. U. S. A.*, 2001, **98**, 10533–10540.
22 L. F. Scatena, M. G. Brown and G. L. Richmond, *Science*, 2001, **292**, 908–912.
23 H. Wang, J. C. Wagner, W. Chen, C. Wang and W. Xiong, *Proc. Natl. Acad. Sci. U. S. A.*, 2020, **117**, 23385–23392.
24 J. Duan, S. Mebs, K. Laun, F. Wittkamp, J. Heberle, T. Happe, E. Hofmann, U.-P. Apfel, M. Winkler, M. Senger, M. Haumann and S. T. Stripp, *ACS Catal.*, 2019, **9**, 9140–9149.
25 M. Senger, S. Mebs, J. Duan, O. Shulenina, K. Laun, L. Kertess, F. Wittkamp, U.-P. Apfel, T. Happe, M. Winkler, M. Haumann and S. T. Stripp, *Phys. Chem. Chem. Phys.*, 2018, **20**, 3128–3140.
26 I. Yakimets, S. S. Paes, N. Wellner, A. C. Smith, R. H. Wilson and J. R. Mitchell, *Biomacromolecules*, 2007, **8**, 1710–1722.
27 C. Ho and J. M. Sturtevant, *J. Biol. Chem.*, 1963, **238**, 3499–3501.
28 K. M. Wilbur and N. G. Anderson, *J. Biol. Chem.*, 1948, **176**, 147–154.
29 K. S. Smith and F. G. Smith, *FEMS Microbiol. Rev.*, 2000, **24**, 335–366.
30 D. M. Kern, *J. Chem. Educ.*, 1960, **37**, 14–23.
31 M. Löwe, M. Kalacheva, A. J. Boersma and A. Kedrov, *FEBS J.*, 2020, **287**, 5039–5067.
32 H. DeMirci, Y. Rao, G. M. Stoffel, B. Vögeli, K. Schell, A. Gomez, A. Batyuk, C. Gati, R. G. Sierra, M. S. Hunter, E. H. Dao, H. I. Ciftci, B. Hayes, F. Poitevin, P.-N. Li, M. Kaur, K. Tono, D. A. Saez, S. Deutsch, Y. Yoshikuni, H. Grubmüller, T. J. Erb, E. Vöhringer-Martinez and S. Wakatsuki, *ACS Cent. Sci.*, 2022, **8**, 1091–1101.
33 R. L. Thurlkill, G. R. Grimsley, J. M. Scholtz and C. N. Pace, *Protein Sci.*, 2006, **15**, 1214–1218.
34 Y. Hirakawa, M. Senda, K. Fukuda, H. Y. Yu, M. Ishida, M. Taira, K. Kinbara and T. Senda, *BMC Biol.*, 2021, **19**, 105.
35 M. L. Zastrow, A. F. A. Peacock, J. A. Stuckey and V. L. Pecoraro, *Nat. Chem.*, 2012, **4**, 118–123.
36 L. A. Rettberg, M. T. Stiebritz, W. Kang, C. C. Lee, M. W. Ribbe and Y. Hu, *Chem.–Eur. J.*, 2019, **25**, 13078–13082.
37 M. Meneghello, A. R. Oliveira, A. Jacq-Bailly, I. A. C. Pereira, C. Leger and V. Fourmond, *Angew. Chem., Int. Ed.*, 2021, **60**, 9964–9967.
38 D. Shevela, H.-N. Do, A. Fantuzzi, A. W. Rutherford and J. Messinger, *Biochemistry*, 2020, **59**, 2442–2449.
39 G. Parkin, *Chem. Rev.*, 2004, **104**, 699–768.
40 L. Koziol, C. A. Valdez, S. E. Baker, E. Y. Lau, W. C. Floyd, S. E. Wong, J. H. Satcher, F. C. Lightstone and R. D. Aines, *Inorg. Chem.*, 2012, **51**, 6803–6812.
41 S. J. Cobb, V. M. Badiani, A. M. Dharani, A. Wagner, S. Zacarias, A. R. Oliveira, I. A. C. Pereira and E. Reisner, *Nat. Chem.*, 2022, **14**, 417–424.
42 S. Kobayashi and K. Manabe, *Acc. Chem. Res.*, 2002, **35**, 209–217.
43 G. Li, B. Wang and D. E. Resasco, *ACS Catal.*, 2020, **10**, 1294–1309.

© 2024 The Author(s). Published by the Royal Society of Chemistry